Title: Synaptic and membrane conductance underlie phase transition in a simple half-center oscillator.

Running Head: Dynamic properties within a half-center oscillator

Authors: Akira Sakurai[1]* and Paul S. Katz[2]

1. Neuroscience Institute, Georgia State University, Atlanta, GA 30302-5030, USA

2. Department of Biology, University of Massachusetts Amherst, Amherst MA 01003, USA

*Corresponding author, Neuroscience Institute, Georgia State University, Atlanta, GA 30302-5030, USA akira@gsu.edu

Number of pages: 28

Number of Figures: 11

Number of Tables: 0

Number of Words:

Abstract: 250

Introduction: 561

Discussion: 1790

Conflict of interest: The authors declare no competing financial interests.

Acknowledgments: This work was supported by NSF grant IOS-1120950.

Abstract (250/250 words)

Rhythmically active neural circuits often contain reciprocally inhibitory modules that act as half-center oscillators. In half-center oscillators, alternating burst discharges require a mechanism to transition activity from one phase to the next, which requires particular synaptic and membrane properties. Here we found that active membrane properties of specific neurons and the temporal dynamics of particular synapses both contribute to the production of a stable rhythmic motor pattern in the swim central pattern generator (CPG) of the nudibranch mollusc, *Dendronotus iris*. This CPG is composed of only four neurons that are organized into two competing modules of a half-center oscillator. Each module is composed of a Swim Interneuron 2 (Si2) and the contralateral Swim Interneuron 3 (Si3). Si2 and Si3 each inhibit their own contralateral counterparts; however, the S2 contralateral synapses have a more negative reversal potential, making them more effective at hyperpolarizing the Si2 and the electrically coupled Si3 of the other module. Si3 rebounds first from inhibition due to a hyperpolarization-activated slow inward current. Si3 excites the Si2 in its module through both chemical and electrical synapses. An Si2-evoked slow inhibitory synaptic potential in Si3 suppresses its firing, terminating the burst generated by the module. Using dynamic clamping, we showed that the magnitude of the slow inhibition sets the periodicity of the oscillator. Thus, the network-driven oscillation is produced by each module rebounding from inhibition, maintaining the burst through self-excitation, and then terminating its burst through a buildup of slow synaptic inhibition, thereby releasing the other module from inhibition.

Keywords: Rhythmogenesis; Gastropod; Locomotion; voltage clamp, Invertebrate

Introduction (561 words)

Since the original proposal of the half-center oscillator (HCO) concept by Bown (1911), reciprocal inhibition between two modules has been considered to be the fundamental architecture of network oscillators (Grillner and El Manira 2015; Kiehn 2016; Moult et al. 2013). However, reciprocal inhibition by itself is not sufficient to maintain stable rhythmic bursting. In many systems, endogenous or conditional bursting properties contribute to maintaining the alternation of half-center oscillators (Arshavsky et al. 1986; Cymbalyuk et al. 2002; Kiehn et al. 1996; Li et al. 2010; Reith and Sillar 1998; Selverston and Miller 1980; Wallen and Grillner 1987). However, a complete mechanistic understanding of network-driven oscillations in a central pattern generator (CPG) is lacking. Here we found that synaptic and membrane properties of identified neurons within each HCO module account for rhythmic bursting activity in the CPG underlying swimming in the nudibranch mollusc, *Dendronotus iris.*

An HCO is composed of a pair of modules that exhibit spiking or bursting activity in alternation through reciprocal inhibition. The reciprocal inhibition is crucial for alternating bursts; however, the network also requires a dynamic property that terminates ongoing excitation in each module so that it can either be released from inhibition or escape from it, and thereby trigger phase transition to the other module (Arbas and Calabrese 1987a; Friesen 1994; Friesen and Stent 1978). Active membrane properties of neurons, such as "sag" depolarization and post-inhibitory rebound, have been shown to be involved in the transition of activity by allowing the postsynaptic neurons to escape from inhibition or firing once released from inhibition (Arbas and Calabrese 1987b; Arshavsky et al. 1985; Dethier et al. 2015; Li and Moult 2012). Studies using computer models also demonstrated the role of the post-inhibitory rebound in escaping from inhibition (Daun et al. 2009; Perkel and Mulloney 1974; Wang and Rinzel 1992).

Another mechanism that assists the activity transition is self-inhibition within each half-center module, which releases the other module from inhibition (Friesen 1994). However, there have been few reports on such self-inhibition playing an essential role in the HCO. In this study,

74 we found a new mechanism of the phase transition. A slow inhibitory synapse within each half-
75 center acts as a feedback inhibition that terminates its own burst to prompt the phase
76 transition to the other half of the HCO.

77 *Dendronotus iris* swims by rhythmically flexing its body alternately from left to right
78 (Sakurai et al. 2011). The rhythmic motor pattern originates from the swim CPG, which consists
79 of only two pairs of interneurons, Si2 and Si3 (Fig. 1A, B) (Sakurai and Katz 2016). Both Si2 and
80 Si3 form reciprocally inhibitory synapses with their contralateral counterparts, forming an HCO
81 (Fig. 1B). The neuronal components (Si2 and Si3) of each HCO module (α and β) are
82 contralateral to each other in the brain; that is, the contralateral Si2 and Si3 fire in phase with
83 each other as a module (Fig. 1C*i*). A strong excitatory synapse from Si3 to Si2 and electrical
84 coupling mediates their synchronous firing in each module (Fig. 1C*ii*). In this study, we
85 investigated the mechanisms underlying the transition of activity between the two modules of
86 the swim CPG. We found that the two neurons in the module each contribute differently to
87 burst initiation and termination on each cycle. Specifically, the combined action of a slow
88 synapse and active membrane properties provide dynamic features needed for this half-center
89 oscillator to function.

Materials and Methods

Animal collection, maintenance, and dissection

Specimens of *Dendronotus iris* (Mollusca; Gastropoda; Nudibranchia), 6-20 cm long, were collected on the Pacific coast of North America by Monterey Abalone Company (Monterey, CA) and Living Elements Ltd (Delta, BC, Canada). The animals were kept in artificial seawater tanks at 10-12°C with a 12:12 light/dark cycle.

Before the surgery for brain isolation, the animal was anesthetized by injecting 0.33 M magnesium chloride solution (20-50 mL) into the body cavity, and an incision was made through the body wall near the esophagus. Then all nerve roots exiting the brain were severed and the brain (Fig. 1A) consisting of the cerebral ganglia, pleural ganglia, and pedunculopontine ganglia were isolated by severing the esophagus. The isolated brain was pinned with the dorsal side up on the bottom of a Sylgard-lined dish and perfused at a rate of 0.5 ml/min with normal saline (mM: 420 NaCl, 10 KCl, 10 CaCl2, 50 MgCl2, 11 D-glucose, 10 HEPES, pH 7.6) or artificial seawater (Instant Ocean, Mentor, OH). The brain was chilled down to 4°C to, and the connective tissue and the brain sheath were removed with forceps and fine scissors. After desheathing, the temperature was raised to 10°C for electrophysiological experiments.

Electrophysiology

Intracellular recordings were performed using 15-35 MΩ glass microelectrodes filled with a solution containing 2 M potassium acetate and 0.2 M potassium. Each electrode was connected to the headstage of the Axoclamp 2B amplifier (Molecular Devices, Sunnyvale, CA). The output signals of the amplifier were digitized at a sampling frequency of >2 kHz using a 1401Plus or Micro1401 A/D converter (Cambridge Electronic Design, Cambridge, UK). Data acquisition and analysis were performed with Spike2 software (CED, Cambridge, UK) and SigmaPlot (Jandel Scientific, San Rafael, CA).

To investigate the effects of depolarization or hyperpolarization of the swim interneurons on the swim rhythm, a positive or negative current pulse (from -4 nA to 4 nA) was injected directly into the neurons via bridge-balanced microelectrodes. In some experiments, spontaneous neuronal activity was suppressed by applying high divalent cation (Hi-Di) saline, which raises the threshold for neuronal spiking. The composition of Hi-Di saline (in mM) was 285 NaCl, 10 KCl, 25 $CaCl_2$, 125 $MgCl_2$, 11 D-glucose, 10 HEPES, pH 7.6. The reversal potentials of synaptic potentials and the strengths of electrical connections were measured by injecting a steady current under discontinuous current-clamp mode or through an additional microelectrode placed in the same neuron. In some experiments, calcium-free Hi-Di saline was used to block chemical synaptic transmission. In low calcium Hi-Di saline, $CaCl_2$ was replaced by $MgCl_2$.

Dynamic clamp

To artificially enhance or counteract the Si2-evoked slow IPSPs in Si3, we performed dynamic clamping with the software StdpC (Kemenes et al. 2011). Each Si3 was impaled with two microelectrodes, one for measuring the membrane potential and the other for injecting current (see Fig. 10Ai). Every time Si2 generates an action potential that exceeded 0 mV, the amount of current injected into the postsynaptic Si3, I_{stim}, was calculated using a first-order kinetics model of the release of neurotransmitter (Destexhe et al. 1994; Kemenes et al. 2011; Sharp et al. 1996):

$$I_{\mathrm{syn}} = g_{\mathrm{syn}}\, S(t)[V_{\mathrm{syn}} - V_{\mathrm{post}}(t)], \qquad \text{(eq. 1)}$$

where $S(t)$ is the instantaneous synaptic activation, g_{syn} is the maximum synaptic conductance, V_{syn} is the reversal potential (-70 mV) of the synapse. To counteract Si2-evoked synaptic potentials, a negative value was used for g_{syn}.

The instantaneous activation, $S(t)$, is given by the differential equation:

$$\left(1 - S_{\infty}\left(V_{\mathrm{pre}}\right)\right)\tau_{\mathrm{syn}}\frac{dS}{dt} = \left(S_{\infty}\left(V_{\mathrm{pre}}\right) - S(t)\right), \qquad \text{(eq. 2)}$$

where

$$S_{\infty}\left(V_{\mathrm{pre}}\right) = \begin{cases} \tanh\left[\frac{V_{pre}-V_{thresh}}{V_{slope}}\right] & if\ V_{pre} > V_{Thresh} \\ 0 & otherwise \end{cases} \qquad \text{(eq. 3)}$$

S_{∞} is the steady-state synaptic activation, and τ_{syn} is the time constant for synaptic decay. The Si2-evoked inhibitory postsynaptic current recorded in Si2 under voltage clamp was 0.94 ± 0.2 sec (mean ± SD, N=5). In this study, τ_{syn} was set to 1.0 sec. V_{pre} is the presynaptic membrane potential of Si3 and V_{thresh} is the threshold potential for the release of neurotransmitter; it was set to the level of 50% height of the smallest Si3 action potentials. The synaptic slope parameter of the activation curve (V_{slope}) was set to 25 mV. g_{syn} was varied between -1000 and 1000 nS.

Statistics

Statistical comparisons were performed using SigmaPlot ver. 12.5 (Jandel Scientific, San Rafael, CA) for Student's *t*-test, paired *t*-test, and Kruskal-Wallis one-way ANOVA on Ranks with all pairwise Multiple Comparison Procedures. Shapiro-Wilk test was used to assume normality of data structure. In all cases, $P<0.05$ was considered significant. For *t*-tests, a two-tailed P value was used. Results are expressed as the mean ± standard deviation (SD).

163

164

165 **Results**

166 *Si2-evoked IPSPs have a more hyperpolarized reversal potential than those of Si3*

167 In the *Dendronotus* swim CPG, two types of neurons, Si2 and Si3, each form inhibitory
168 reciprocal synapses with the contralateral analog. To compare the strength of these synapses,
169 we suppressed spontaneous activity using high divalent cation (Hi-Di) saline, which raises the
170 spike threshold and thereby minimizes spontaneous and polysynaptic activity. We found that
171 the reversal potentials of these inhibitory synapses differ (Fig. 2); the average reversal potential
172 of Si2-to-SI2 IPSPs was -73.9 ± 8.1 mV (N = 5; Fig. 2A*i*, B), whereas the Si3-to-Si3 IPSP reversal
173 potential was -46.4 ± 3.9 mV (N = 4; Fig. 2A*ii*, B). This indicates that, near the resting potential
174 (about -50 mV), the inhibitory synapse of Si2 would greatly hyperpolarize the postsynaptic Si2,
175 whereas the inhibitory synapse of Si3 would hardly change the membrane potential of the
176 postsynaptic Si3 but only increase the membrane conductance. This also suggests that the
177 inhibitory synapses between the Si3 pair differ from that of the Si2 pair in the ionic basis of
178 their postsynaptic currents.

179

180 *Si2 evokes a larger inhibitory effect on the opposite module than Si3.*

181 During the swim motor pattern, both Si2 and Si3 receive rhythmic synaptic inhibition from their
182 contralateral counterparts. To better evaluate the contributions of Si2 and Si3, we stimulated
183 each independently (Fig. 3). A train of action potentials in Si2 produced a brief
184 hyperpolarization and a delayed depolarization in the Si2 and Si3 of the opposite module (Fig.
185 3A). The depolarization led to a burst discharge in Si3. Similar post-inhibitory rebound
186 discharges in Si3 were seen in all preparations examined (100%, N = 28). In 68% of
187 preparations, the contralateral Si2 also showed the post-inhibitory rebound discharge (N = 19
188 of 28), which were all triggered by the Si3-evoked EPSPs (Fig. 3A, asterisks).

189 In contrast, a similar train of action potentials in Si3 evoked only small synaptic
190 potentials in Si2 and Si3 of the opposite module. Rebound firing in the contralateral Si3

occurred in 69% of preparations (N=11 of 16), which induced the ipsilateral Si2 firing in 43.8% of preparations (N = 7 of 16). Thus, an Si2 spike train induced a rebound discharge of Si3 in the opposite module more frequently than the Si3-induced discharge. These results show that the inhibitory synaptic inputs from Si2 not only provide inhibition to the other half-center module but also induce an excitatory response in Si3 via post-inhibitory rebound excitation.

The difference in the size of the evoked inhibition was more pronounced in Hi-Di saline (Byrne et al. 1978; Liao and Walters 2002; Sakurai and Katz 2003; Sakurai et al. 2011), which raises spike threshold and thereby minimizes spontaneous and polysynaptic activity (Fig. 4). A 10Hz spike train in the L-Si2 produced a 10mV hyperpolarization of the R-Si2 (N=21, Fig. 4A). The L-Si3 was also hyperpolarized because it is electrically coupled to the R-Si2 (Sakurai and Katz 2016). The mean amplitude of the IPSP evoked by a 10-Hz spike train of Si2 was -12.3 ± 1.6 mV (N = 7) in the contralateral Si2 and -7.0 ± 2.0 mV (N = 6) in the ipsilateral Si3 (Fig. 4C). In contrast, a 10Hz spike train in the R-Si3 produced just a small hyperpolarization in both neurons of the other module (N = 19, Fig. 4B); the mean IPSP amplitudes were only -2.0 ± 1.9 mV (N = 5) in the contralateral Si3 and 1.4 ± 1.0 mV (N = 7) in the ipsilateral Si2 (Fig. 4C). Thus, Si2 evoked larger inhibitory potentials than Si3 in neurons of the other module.

Si3, not Si2, exhibits a post-inhibitory rebound

Immediately after the Si2 stimulation, the membrane potential of the contralateral Si2 in the other module slowly returned to its original resting potential (R-Si2 in Fig. 4A), while Si3 not only recovered more quickly but also showed a rebound depolarization that exceeded the original membrane potential (L-Si3 in Fig. 4A, asterisk). Neither neuron exhibited rebound depolarization when Si3 was stimulated (Fig. 4B). The rebound depolarization induced by Si2 onto the ipsilateral Si3 in the other module was significantly larger than any other synapses (Fig. 4D, $P<0.05$ by Kruskal-Wallis one-way ANOVA on Ranks with all pairwise multiple Comparison Procedures). The post-inhibitory rebound depolarization was largest in Si3 than Si2.

217 Si3 exhibited a larger post-inhibitory rebound depolarization following hyperpolarizing
218 current steps than Si2 (Fig. 5). In normal saline, injection of a hyperpolarizing current pulse (1-4
219 nA, 4 sec) into Si2 produced only a hyperpolarizing potential change with little or no spike
220 discharges afterward (Fig. 5A, left). In contrast, a hyperpolarizing current pulse in Si3 caused a
221 post-inhibitory rebound discharge upon its termination of the pulse (Fig. 5A, right). The number
222 of spikes after the current injection pulse was significantly larger in Si3 than Si2 (Fig. 5B; $P <$
223 0.001 by Two-way repeated-measures ANOVA with Holm-Sidak method, N = 9-12 for Si2 and N
224 = 8-10 for Si3). When the spike threshold was raised by Hi-Di saline, Si3 showed a depolarizing
225 overshoot when released from the hyperpolarizing current injection (Fig. 5C). This rebound
226 potential was significantly larger in Si3 than Si2 (Fig. 5D; $P < 0.001$ by Two-way repeated-
227 measures ANOVA with Holm-Sidak method, N = 20-23 for Si2 and N = 19-21 for Si3).

228

229 *Si3 exhibits a hyperpolarization-activated inward current*

230 In addition to the rebound excitation, both Si2 and Si3 exhibited a "sag" potential
231 during the hyperpolarizing current injection (Fig. 5A, C). Although the difference in the
232 magnitude of this sag potential was less prominent than the rebound potential, there was a
233 significant difference in the responses caused by a -4 nA current pulse (Fig. 5E; $P < 0.001$ by
234 Two-way repeated-measures ANOVA with Holm-Sidak method, N = 23 for Si2 and N = 21 for
235 Si3).

236 Under voltage clamp, Si3, but not Si2 exhibited a hyperpolarization-activated inward
237 current (Fig. 6). Step-wise hyperpolarizing changes of membrane potential did not produce a
238 noticeable current response in Si2, whereas in Si3 it evoked a slow inward current (Fig. 6A). The
239 amplitude of the inward current increased in proportion to the hyperpolarizing voltage steps
240 (Fig. 6B).

241 Together, these results suggest that Si2 and Si3 have distinct membrane properties. The
242 hyperpolarization-activated slow inward current in Si3 likely underlies the sag depolarization
243 and subsequent rebound depolarization, which produces the post-inhibitory rebound discharge

244 in Si3 and consequently induces the phase transition from one module of the half center to the
245 other.

246

247 *Si2 provides a burst-limiting mechanism within each half-center module*

248 We previously demonstrated that strong excitatory coupling between Si2 and the
249 contralateral Si3 via an excitatory synapse and electrical coupling causes them to fire together
250 as a half-center module (Sakurai and Katz 2016). Here we found that Si2 also evokes a slow
251 inhibitory synaptic action on Si3 (Fig. 7A). Although the Si2-to-Si3 electrotonic connection
252 contributes to enhanced spiking within the module, the excitation was always overwhelmed by
253 delayed inhibition that suppressed spiking in Si3 (Fig. 7A,B).

254 When the spike threshold was increased in Hi-Di saline, an Si2 spike train produced a
255 one-for-one electrotonic EPSPs in the contralateral Si3 (Fig. 7B*i*). With increased spike
256 frequency, a slow hyperpolarizing potential counteracted the electrotonic EPSPs and produced
257 an overall hyperpolarization (Fig. 7B*i*, 10 Hz).

258 The application of Ca^{2+}-free saline blocked this hyperpolarization without changing the
259 electrotonic EPSPs (Fig. 7B*ii*, C). Subtracting traces in Ca^{2+}-free saline (Fig. 7B*ii*) from those in Hi-
260 Di saline (Fig. 7B*i*) revealed the Ca^{2+}-sensitive component of the Si2-evoked postsynaptic
261 potential in Si3 (Fig. 7B*iii*). These results suggest that this slow inhibition was mediated by
262 chemical neurotransmitter release.

263 Under voltage clamp, a spike train in Si2 produced a slow inhibitory postsynaptic current
264 (IPSC) in the contralateral Si3 (Fig. 8A). The amplitude of the slow IPSC was outwardly rectifying.
265 The reversal potentials were variable across individuals ranging from -60 to -80 mV (Fig. 8B).
266 The time constant of the falling phase of the slow IPSP was 0.94 ± 0.2 sec (N = 5). During the Si2
267 spike train, the membrane conductance of Si3 increased in all three preparations examined
268 from an average of 80.7 ± 15.3 nS to 141 ± 22.1 nS (P = 0.039 by paired *t*-test, N = 3). The
269 outward rectification of the slow IPSC was not likely due to a change in background membrane

conductance via opening or closing of voltage-gated channels because the input resistance of each cell was constant throughout the voltage range examined (Fig. 8C). At present, it is unclear how such apparent outward rectification was brought about. The variability in the reversal potential and the non-linearity of the I-V relationships could also be an experimental artifact caused by poor space clamping, suggesting that the synapse is located contralateral to the Si3 soma.

Feedback inhibition from Si2 to Si3 contributes to burst termination

To determine the role that the inhibition from Si2 to the contralateral Si3 plays in rhythmic burst generation, we examined the effect of suppressing spikes in Si2 during the swim motor pattern (Fig. 9). When unperturbed, the intra-burst spike frequency of Si3 showed an initial peak and a subsequent steep decline during each burst (Fig. 9A,B, burst *a*). Suppression of spiking in Si2 by hyperpolarizing current injection increased the duration of Si3 bursts immediately (Fig. 9A,B burst *b*). The duration of the Si3 burst during the swim motor pattern increased significantly from 2.7 ± 0.9 sec to 4.1 ± 1.1 sec when the Si2 in its module was hyperpolarized (Fig. 9C*i*; $P < 0.001$ by two-tailed paired t-test, N=12). The duty cycle of Si3 burst increased significantly from 0.54 ± 0.09 to 0.67 ± 0.13 with the Si2 hyperpolarized (Fig. 9C*ii*; $P < 0.001$ by Wilcoxon Signed Rank Test, N = 12). The Si2 hyperpolarization also caused a significant increase in the number of Si3 spikes from 19.5 ± 4.9 to 28.4 ± 9.3 ($P < 0.001$ by two-tailed paired t-test, N = 12) (Fig. 9C3). These results suggest that Si2 has two opposing actions on the Si3 in its module: 1) it enhances the Si3 burst through an electrotonic synapse, and 2) it slowly decreases Si3 firing through a chemical inhibitory synapse.

293 *Dynamic clamp manipulation of slow inhibitory synapses revealed its role in the burst frequency*
294 *of the swim motor pattern*

295 The results suggest that the slow inhibition from Si2 to Si3 in each module decreases Si3
296 firing and hence decreases the excitatory drive on Si2. We hypothesized that the self-inhibition
297 within the module helps to terminate the burst and transition to activation of the other
298 module. To test this, we artificially enhanced or reduced the magnitude of the inhibition from
299 Si2 to Si3 in both modules during a swim motor pattern using the dynamic clamp technique.
300 The amplitudes and time courses of the Si2-evoked synaptic currents were calculated in real-
301 time (Fig. 10A*i*, see Materials and Methods) and injected into Si3 through the recording
302 electrode in response to spikes in the contralateral Si2. While the dynamic clamp was engaged,
303 an Si2 burst set off a slow negative current injected into Si3, boosting the slow inhibitory
304 synapse, which shortened the Si3 burst (Fig. 10A*ii*). Spikes in the postsynaptic Si3 also produced
305 spike-like downward surges in the injected current because the spikes moved the membrane
306 potential away from the reversal potential of the slow IPSC (-70 mV).

307 Augmenting the amplitude of the slow inhibitory synaptic conductance at the Si2-to-Si3
308 synapse shortened the Si3 burst duration, thereby decreasing the burst period (Fig. 10B,D). In
309 contrast, counteracting the inhibition with an inverted conductance reduced the Si2-to-Si3
310 inhibition and extended Si3 bursts, thereby increasing the burst frequency (Fig. 10C,D). Thus,
311 the feedback inhibition from Si2 to Si3 within the module plays a crucial role in maintaining the
312 periodicity of the half-center oscillator.

313

314 **Discussion**

315 In this study, we identified the synaptic and membrane conductances that contribute to the
316 stable alternations underlying the *Dendronotus* swim motor pattern. Specifically, we found that
317 slow inhibitory synaptic connection within each module acts as a self-limiting mechanism to
318 halt the excitatory synaptic drive. This, in turn, causes a transition of excitation from one side to

319 the other. Moreover, the neurons that receive the slow synaptic inhibition exhibit membrane
320 properties that cause post-inhibitory rebound firing that is triggered following release from
321 inhibition by the other module.

322 The actual sequence of activity in the *Dendronotus* swim CPG circuit is as follows (Fig.
323 11): Si2 and the contralateral Si3 in Module α fire synchronously through excitatory synapses
324 and electrical coupling (a). As Si2 exerts a slow synaptic inhibition on Si3, the spike frequency of
325 Si3 gradually decreases, lessening the excitatory drive to Si2 (b). Concurrently Module α Si2
326 inhibits its contralateral counterpart in Module β. Cessation of spiking in Module α leads to
327 post-inhibitory rebound of Si3 in Module β. The firing of the Module β neurons suppresses the
328 activity of the Module α, and hence the transition of excitation occurs (c). Slow inhibitory
329 feedback in Module β weakens the Si3 activity until Module α rebounds (d).

330

331 *The role of active membrane properties the swim CPG*

332 Si3 neurons, but not Si2 neurons, showed post-inhibitory rebound when it was released from
333 hyperpolarization or after a train of IPSPs evoked by the other half-center module. The post-
334 inhibitory rebound property is present in many neural circuits with the half-center
335 configuration; it plays a crucial role in the maintenance of rhythmic neural activity by prompting
336 the transition of activity phases from one side to the other (Angstadt et al. 2005; Arshavsky et
337 al. 1998; Dethier et al. 2015; Li and Moult 2012; Nagornov et al. 2016; Pirtle and Satterlie 2007;
338 Pirtle et al. 2010; Roberts et al. 2008; Rodriguez et al. 2013). For example, in tadpoles, the firing
339 of excitatory descending interneurons is triggered by a post-inhibitory rebound. The rebound
340 occurs when the membrane is held in a depolarized state by sustained excitatory input and
341 then hyperpolarized by inhibitory input (Li et al. 2007; Roberts et al. 2008). Computer models of
342 the half-center oscillator have demonstrated the contribution of a post-inhibitory rebound in
343 phase transitions (Daun et al. 2009; Dethier et al. 2015; Wang and Rinzel 1992).

344 Before the rebound discharge, both Si2 and Si3 neurons showed a sag potential that
345 gradually depolarizes the membrane. This time-dependent change in membrane potential may

346 contribute to the escape of these neurons from synaptic inhibition by the contralateral half-
347 center module (Arbas and Calabrese 1987b; Pirtle et al. 2010). It has been well acknowledged
348 that a hyperpolarization-activated inward current and a low-threshold T-type calcium current
349 contribute to rebound responses in both vertebrates and invertebrates (Angstadt et al. 2005;
350 Dethier et al. 2015). The contribution of hyperpolarization-activated sodium current (Nadim et
351 al., 1995) and persistent sodium current (McCrea and Rybak 2008; Tazerart et al. 2007; Zhong
352 et al. 2007; Ziskind-Conhaim et al. 2008) to the sag potential has also been shown. These
353 observations suggest that sag potentials and post-inhibitor discharges contribute substantially
354 to the transition of activity in the Dendronotus swim CPG. Interestingly, of the two cell types
355 that make up the half-center, the post-inhibitory rebound property was found only in Si3 but
356 not in Si2. It is currently unclear which ion permeability underlies the sag and the rebound
357 discharge in Si3 neurons. In the previous study, we have shown that the central command
358 neuron, Si1, makes synapses onto Si3 and potentiates the Si3 synaptic strength (Sakurai and
359 Katz 2019). The modulatory effects of Si1 on the membrane excitability of Si3 are of interest
360 and remain to be investigated in the future.

361

362 *Differentiation of the role inhibitory synaptic actions onto the contralateral module*

363 Although both Si2 and Si3 have reciprocal inhibitory synapses with their contralateral
364 counterparts, as is typical for a half-center oscillator, the results of this study show that their
365 synaptic properties are different. Specifically, the Si2-evoked IPSPs in the contralateral Si2 had a
366 reversal potential at a more hyperpolarized level than that of Si3, which results in a larger IPSP
367 than the Si3-Si3 synapse. The Si2-evoked IPSPs in the contralateral Si2 caused a
368 hyperpolarization in Si3 in the same module via electrical coupling, which leads to a post-
369 inhibition rebound firing in the Si3. In contrast, Si3-evoked IPSPs had a reversal potential near
370 the resting potential, and therefore, their inhibitory effect is not due to membrane
371 hyperpolarization but to shunting inhibition caused by an increase in membrane conductance
372 (Paulus and Rothwell 2016), which has little effect on the voltage-dependent channels that

373 underlie the induction of rebound discharge. As described later, Si2 also provides inhibitory
374 feedback to Si3 within the same half-center module. Thus, the inhibitory synapse of Si2 is
375 responsible for stopping the activity of Si3 in the same module while triggering rebound firing
376 of Si3 in the contralateral module. This is in stark contrast to the excitatory synapse of Si3,
377 which triggers the excitation of Si2. These facts indicate that there is a functional differentiation
378 between the inhibitory synaptic functions of Si2 and Si3 neurons, which is reflected in their
379 ability to induce a post-inhibitory rebound.

380

381 *The role of self-inhibition in the rhythmogenesis*

382 The key finding of this study is the discovery of a synaptic mechanism that serves as a brake on
383 self-excitation within each module of the half-center circuit. In a previous study, we described
384 that Si2 and Si3 are strongly linked by excitatory synapses and electrical connections in each
385 half-center of the *Dendronotus* swim CPG. The resulting synchronized activity is essential for
386 maintaining half-center oscillator activity (Sakurai and Katz 2016). Here, we found that Si2 also
387 inhibits Si3 and that this slow synaptic action acts as feedback inhibition to limit the burst
388 duration.

389 In the original concept of the half-center oscillator, it was originally thought that the
390 reciprocal inhibition between two half-center modules was essential for alternating rhythm generation
391 and that endogenous rhythmogenesis in each module is not required (Brown 1911). However, without
392 a mechanism that prompts the transition of activity from one side to the other, the module in
393 one side would remain active for an extended period of time while the other side is inhibited.
394 Friesen (1994) suggested that one potential mechanism that could provide a dynamic property
395 to the half-center oscillator is spike frequency adaptation which limits the duration of excitation
396 in one module, ensuring that a pair of mutually inhibitory neurons acts as an alternating
397 oscillator rather than a bistable switch. However, few such circuits have been reported. Instead,
398 neural circuits with a half-center configuration often are capable of generating endogenous bursting
399 upon isolation (Arshavsky et al. 1986; Cymbalyuk et al. 2002; Selverston and Miller 1980). Similar

400 conditional pacemaker properties also have been found in each half of the locomotor circuit in the
401 spinal cord (Kiehn et al. 1996; Li et al. 2010; Reith and Sillar 1998; Wallen and Grillner 1987). When the
402 left and right modules of the spinal swimming circuit are separated in lamprey, each module exhibits
403 rhythmic bursting activity at a faster rhythm than normal (Grillner 2003). If each half-center possesses
404 endogenous rhythmogenesis, then the role of mutual inhibition between half-centers is limited to
405 ensuring coordinated bursts in alternation (Ausborn et al. 2018; Hagglund et al. 2013). A
406 counterexample to this was reported by Moult et al. (2013), in which they showed that the onset of
407 rhythmic activity did not occur instantaneously when unilateral activity is momentarily inhibited but
408 took some time, suggesting that some neuroplasticity may be involved in the experimentally induced
409 onset of unilateral automaticity (Moult et al. 2013). In *Dendronotus*, it is unlikely that each module of
410 the swim CPG has rhythmogenesis, because no oscillatory activity was seen when the activity of one side
411 was suppressed by current injection (Sakurai and Katz 2016). The Si3 pair alone cannot generate
412 oscillatory activity even though they were depolarized by current injection. Thus, the *Dendronotus* swim
413 CPG is a unique example of a network oscillator in half-center configuration, where each half-center has
414 no rhythmogenesis. Instead, the recurrent feedback synapse within each half-center module, the
415 escaping from inhibition by sag depolarization, and subsequent post-inhibitory rebound are essential for
416 rhythm generation by prompting the activity transfer from one side to the other.

417

418 *Comparisons to the Melibe swim CPG*

419 Another nudibranch, *Melibe leonina*, swims with rhythmic left-right body flexions like
420 Dendronotus, and the details of its swim circuits have been well-elucidated (Sakurai et al. 2014;
421 Sakurai et al. 2011; Watson et al. 2002). The swim CPG of *Melibe* consists of four pairs of
422 interneurons, each forming a half-center configuration with reciprocal inhibition similar to
423 *Dendronotus*, but it has more complex synaptic interaction networks than that of *Dendronotus*
424 (Sakurai et al. 2014). In *Melibe*, multiple synaptic inputs acting in succession are essential for
425 the transition of activity from one side of the swim CPG to the other. In the *Melibe* swim CPG,
426 the primary half-center kernel, consisting of Si1 and Si2, generates alternating burst discharges.
427 The burst discharge in one side of the primary half-center kernel is terminated by the inhibitory
428 synaptic input from the secondary half-center kernel, Si3, which fires with a 25% delay from the

429 primary kernel. On the other hand, it is the inhibitory synaptic input of Si2 and Si4 in the first
430 kernel that triggers and terminates the group discharge of Si3 in the second kernel and triggers
431 the transition of activity. Meanwhile, Si1, Si2, and Si4 of the primary kernel trigger and
432 terminate the burst discharge of Si3, and hence trigger a transition of activity in the secondary
433 kernel. Thus, despite showing similar swimming behaviors and have some homologous
434 neurons, the mechanisms underlying the generation of the motor pattern are substantially
435 different between these two nudibranch species. In *Melibie*, the primary and secondary half-
436 center kernels promote the transition of each other's activity, which contrasts with that of
437 *Dendronotus*, in which burst discharge is terminated by a feedback mechanism within each side
438 of a single half-center kernel.

439

440 *Conclusion*

441 The present study demonstrated how a transition of excitation from one side to the other in a
442 simple CPG with a half-center configuration. The transfer of excitation is prompted through the
443 combined action of feedback inhibitory synapses and active membrane properties within each
444 half-center module: the self-termination of a burst by the recurrent inhibition, the strong
445 inhibitory input from the other half-center, escape from hyperpolarization by the sag potential,
446 and the rebound discharge upon release from inhibition. Thus, even in the half-center
447 oscillator, which is said to be the simplest building block of the neural circuit, many functional
448 factors overlap and act to produce a stable rhythm. It is of interest how two different neural
449 circuit mechanisms diverged from their common ancestor.

450 **Figure Legends**

451 **Figure 1.**

452 The central pattern generator (CPG) underlying the swimming behavior of *Dendronotus iris*. ***A***.
453 Schematic drawing of the cell body locations and the axonal projections of the swim CPG
454 neurons, Si2 (blue) and Si3 (red), in the *Dendronotus* brain, showing Cerebral, Pleural, and two
455 Pedal (proximal and distal) ganglia based on Sakurai and Katz (2016). Si2 and Si3 have their cell
456 bodies in the proximal pedal ganglion. They each project an axon to the contralateral pedal
457 ganglion through one of the two pedal-pedal commissures. Only L-Si2 and R-Si3 axon
458 projections are depicted. Each module of the half-center oscillator that constitutes the
459 swimming circuit is composed of Si2 and Si3 with cell bodies on opposite sides. ***B***. The
460 previously published connectivity of the *Dendronotus* swim CPG. Lines terminating in triangles
461 indicate excitatory synapses, filled circles inhibitory synapses. Resistor symbols indicate
462 electrical connections. We named each half-center module, module α and β. Module α consists
463 of left Si2 and right Si3, and module β consists of right Si2 and left Si3. ***C***. The swim motor
464 pattern recorded intracellularly from all four swim interneurons (***Ci***). Si2 and Si3 in the same
465 module burst together via an excitatory synapse and an electrical connection. The two modules
466 exhibit alternating bursts. A portion of the traces indicated by the dotted box is enlarged in ***Cii***.
467

468 **Figure 2.**

469 The inhibitory synaptic potentials generated by Si2 and Si3 have different reversal potentials. ***A***.
470 Schematic diagrams of synaptic connections in the swim CPG and reversal of Si2-to-Si2 (***Ai***) and
471 Si3-to-Si3 (***Aii***) synaptic potentials. Spikes in the presynaptic L-Si2 and L-Si3 and the resulting
472 postsynaptic potentials in the contralateral R-Si2 (***Ai***) and L-Si3 (***Aii***) were recorded in Hi-Di
473 saline. One electrode was inserted into L-Si2 (***Ai***) or R-Si3 (***Aii***) to record the presynaptic action
474 potentials, while two electrodes (one for voltage recording and the other for current injection)
475 inserted into R-Si2 (***Ai***) or L-Si3 (***Aii***), respectively. Positive or negative current was injected into
476 the postsynaptic cell (R-Si2 or L-Si3) to change its membrane potential. The numbers on the left
477 side of the traces indicate the membrane potential, and ten traces were overlaid for each

478 voltage level. Traces were triggered at the peak of presynaptic action potentials. ***B***. The
479 relationships between the amplitude of the IPSPs and the membrane potential of the
480 postsynaptic cell are shown. The values used are derived from the data shown in ***A***. The white
481 circles indicate the Si2-evoked IPSPSs in the contralateral Si2, and the gray circles are the Si3-
482 evoked IPSPs in the contralateral Si3.
483

484 **Figure 3.**
485 A Si2 spike train causes a post-inhibitory rebound discharge in Si3 of the contralateral module.
486 ***A***. A spike train of about 10 Hz in Si2 produced hyperpolarizing responses in Si2 and Si3 of the
487 other module, followed by post-inhibitory discharges in Si3. From top to bottom, the circuit
488 schematic, membrane potential traces (R-Si2, L-Si3, and L-Si2), and an instantaneous spike
489 frequency plot are shown. Recorded neurons are drawn in black in the top schematic. A current
490 pulse of 4 nA was injected into L-Si2 to evoke a train of spikes at around 10 Hz. ***B***. A current
491 pulse of 3 nA was injected into R-Si3 to evoke a train of spikes at around 10-14 Hz, which
492 produced only small hyperpolarization in the neurons of the other module but evoked no
493 rebound discharge.
494

495 **Figure 4.**
496 A Si2 spike train causes a sag depolarization and a post-inhibitory rebound depolarization in
497 postsynaptic Si3. ***A***. A 10-Hz spike train in Si2 in module α produced hyperpolarization of both
498 Si2 and Si3 in module β. After the stimulation, the membrane potential of the postsynaptic Si2
499 slowly recovered back to the resting potential, whereas Si3 showed a faster recovery and a
500 rebound depolarization (asterisk), which lasted for 10 to 15 sec. The spike train was evoked by
501 injecting repetitive current pulses (10 nA, 20 msec) at 10 Hz. ***B***. A 10-Hz spike train in Si3 in
502 module α produced hyperpolarization of both Si2 and Si3 in module β. The amplitude of
503 hyperpolarization was smaller than those evoked by Si2 in A, and there was no rebound
504 depolarization after the stimulus. The prefixes "*c*" and "*i*" for Si2 and Si3 in parentheses stand
505 for "contralateral" and "ipsilateral". ***C***. Graph comparing the amplitudes of the Si2- and Si3-

506 evoked hyperpolarization in the neurons (*c*Si2, contralateral Si2; *i*Si3, ipsilateral Si3; *c*Si3,
507 contralateral Si3; *i*Si2, ipsilateral Si3) in the other module. ***D***. Graph comparing the amplitude of
508 the post-inhibitory rebound depolarization.

509

510 **Figure 5**

511 Si3 showed remarkable sag and a rebound depolarization. ***A***. Membrane potential responses
512 (upper traces) of Si2 and Si3 to a hyperpolarizing current pulse (-4 nA for 4 sec, lower trace) in
513 normal saline. ***B***. Graph comparing the numbers of spikes in Si2 (black) and Si3 (gray) evoked
514 after the hyperpolarizing current pulses (-1, -2, -3, and -4 nA). Each bar represent mean±SD
515 (Si2, N = 9-12; Si3, N = 7-10). The asterisk indicates significant difference (see text). ***C***.
516 Membrane potential responses (upper traces) of Si2 and Si3 to a hyperpolarizing current pulse
517 (lower trace) in Hi-Di saline. The traces are overlaid. ***D***. Graph comparing the amplitude of
518 rebound depolarization in Si2 (black) and Si3 (gray) after the hyperpolarizing current injection (-
519 1 to -4 nA, 4 sec). The amplitude represents the height from the resting membrane potential to
520 the peak of the rebound depolarization. The asterisk indicates significant difference (see text).
521 ***E***. Graph showing the amplitude of sag depolarization in Si2 (black) and Si3 (gray) during the
522 hyperpolarizing current injection (-1 to -4 nA, 4 sec). The amplitude represents the change in
523 membrane potential from the bottom to the most depolarized potential during the stimulation.
524 The asterisk indicates significant difference (see text).

525

526 **Figure 6**

527 Si3 showed a hyperpolarization-induced inward current. ***A***. Membrane current responses (upper
528 traces) and command voltage pulses (bottom traces). The membrane potential of Si2 or Si3
529 were held at -50 mV under voltage clamp and then were stepped down to more hyperpolarized
530 potentials (from -60 to -90 mV). Each neuron was impaled with two electrodes (one for voltage
531 recording and the other for current injection). All voltage-clamp experiments were performed in

532 Hi-Di saline. ***B***. The amplitudes (nA, mean±SD; Si2, N=5; Si3, N = 8) of membrane current are
533 plotted against the command voltage values (mV).

534

535 **Figure 7**

536 A spike train in Si2 evokes a slow inhibitory synaptic potential in Si3 in the same half-center
537 module. ***A***. An Si2 spike train inhibited ongoing spiking activity of Si3. Traces show the
538 membrane potential activity of Si2 and Si3 and the injected current traces. Tonic spiking in Si3
539 was evoked by injecting 1-nA current pulse (lower traces), during which an intense spiking was
540 evoked in Si2 by injecting 2-nA current pulse (upper traces). The spike train in Si2 inhibited
541 spiking of Si3 in the same module. The schematic on the left shows synaptic interactions
542 between Si2 and Si3 within a half-center module. ***B***. A spike train of Si2 (upper trace) produced
543 complex membrane potential responses of Si3 (lower trace) in the same half-center module,
544 part of which was mediated by chemical transmitter release. Trains of action potentials in R-Si2
545 were evoked by injecting repetitive current pulses (7-15 nA, 20 msec) at 2, 5, and 10 Hz in Hi-Di
546 saline. The Si2 spikes produced sharp electrotonic EPSPs in L-Si3, which overrode on a slow
547 hyperpolarizing potential (***B1***). Ca^{2+}-free saline blocked the slow hyperpolarizing potential,
548 leaving the electrotonic EPSPs relatively unchanged (***B2***). The wavefroms of B2 minus the
549 waveforms of B1 are shown in ***B3***, revealing a slow hyperpolarizing component that was largely
550 blocked by the Ca^{2+}-free saline. ***C***. Graphs showing the amplitude of electrotonic EPSPs (upper
551 graph) and the slow hyperpolarizing potentials (slow IPSPs; lower graph) recorded in Hi-Di saline
552 (black bars) and in Ca^{2+}-free Hi-Di saline (white bars). Ca2+-free saline largely diminished the
553 slow IPSPs but had little effect on the electrotonic EPSPs.

554

555 **Figure 8**

556 The Si2-evoked slow IPSP in the contralateral Si3 is mediated by an outward current. ***A***.
557 Example traces of the synaptic currents at different holding potentials. Spike trains were evoked
558 in R-Si2 by injecting repetitive current pulses (10 nA, 20 msec) at 10 Hz. Seven traces of the Si2

559 spike trains are overlaid and shown at the top, whereas the slow IPSPs in L-Si3, which was
560 voltage-clamped at various potential levels, are shown below. The holding potentials (from -90
561 mV to -30 mV) are shown on the left side of the trace. ***B***. The relationship between the
562 amplitudes of the slow IPSPs and the holding potential of the postsynaptic Si3. The IPSC became
563 outward current with more depolarized holding potential. With more depolarized holding
564 potentials, the amplitudes of the slower IPSCs becomes larger. ***C***. Si3 did not exhibit voltage-
565 dependent current but was passive, and the IV relationship was linear with the holding
566 potentials used in this voltage-clamp experiment.
567

568 **Figure 9**

569 Suppression of the Si2 spike resulted in a prolonged Si3 burst. ***A***. Simultaneous intracellular
570 recording of an Si2 pair and L-Si3. A plot of instantaneous spike frequency is shown at the
571 bottom. From the time indicated by the arrow, a hyperpolarizing current of -4 nA was applied to
572 suppress the action potential of R-Si2. During hyperpolarization, only trains of EPSPs evoked by
573 the L-Si3 spikes were seen in R-Si2. The bursts before and during the hyperpolarizing current
574 injection are boxed by blue (a) and red (b) dotted lines. The spike frequency during the period is
575 indicated by the same color in the plot below. ***B***. A comparison of bursts before and during the
576 hyperpolarizing current injection. Traces ***a*** and ***b*** show the waveforms with a faster timescale of
577 bursts indicated by the boxes in ***A***. The dotted lines indicate 0 mV. Plots of the instantaneous
578 spike frequencies of two bursts are shown below. C. Graphs of burst duration (C1), burst duty
579 cycle (C2), and the number of Si3 spikes per burst before (blue) and immediately after (red) the
580 suppression of the Si2 spikes by hyperpolarizing current injection. All three factors increased
581 when the Si2 spikes were suppressed.
582

583 **Figure 10**

584 Artificial enhancement or suppression of slow inhibitory synaptic action of Si2 onto Si3 within
585 each half-center module changed the burst period of CPGs. ***A***. The experimental arrangement
586 for dynamic clamp is shown (***A1***, see Materials and Methods for details). Every time the

587 membrane potential (V_m) of Si2 surpassed a specified threshold (50% of spike height), an
588 artificial synaptic current (I_{Stim}) was calculated by the computer and injected into the
589 contralateral Si3 to boost the existing Si2-to-Si3 slow synapse (red). Traces in ***A2*** show the
590 change in the burst before and during the application of dynamic clamp. The red arrow
591 indicates the time of onset of dynamic clamping. The red arrow indicates the time when the
592 dynamic clamp was started. The horizontal dotted lines show 0 mV. ***B***. Simultaneous
593 intracellular recording from all four neurons shows the effect of dynamic clamping (red bar).
594 The synaptic boost caused by adding artificial synaptic conductance (500 nS) with the dynamic
595 clamping accelerated the swim motor pattern by shortening the duration of bursts. ***C***. Synaptic
596 suppression by counteracting IPSPs with a negative postsynaptic conductance to Si3 extended
597 the burst duration and consequently increased the burst period. ***D***. Plot of burst periods against
598 the conductance of artificial synapses from Si2 to Si3 in the same half-center module. Boosting
599 the synaptic conductance reduced the burst period, whereas counteracting it extended the
600 burst period.
601
602 **Figure 11**
603 Sequence of activities of the CPG neurons. ***A***. The activity of a circuit neuron is divided into four
604 parts (a, b, c, d): In phase a, Si3 in module α starts firing, and Si2, which is driven by Si3, starts
605 firing a little later. The firing frequency of Si2 and Si3 in module α starts to decline in phase b. At
606 some point, Si3 in module β escapes from inhibition and starts firing together with Si2 (phase c).
607 As a result, the burst of module α ends and the activity switches. The activities of the module β
608 neurons eventually decrease (phase d). ***B***. Schematic diagram of the activity sequence of the
609 CPG neurons. In phase a, Si2 and Si3 in module α fire together through an excitatory synapse
610 and an electrical coupling. They inhibit module β through inhibitory synapses. The firing of Si2
611 gives inhibitory feedback to Si3, and the activity of both decreases (phase b), which weakens
612 the inhibitory synaptic action on module β. Then, two neurons in module β fire together,
613 inhibiting module α (phase c). Eventually, the activity of Si2 and Si3 in module β declines,
614 becoming ready for the transition of excitation back to module α (phase d).

615 **References**

616 **Angstadt JD, Grassmann JL, Theriault KM, and Levasseur SM**. Mechanisms of postinhibitory rebound
617 and its modulation by serotonin in excitatory swim motor neurons of the medicinal leech. *J Comp*
618 *Physiol A Neuroethol Sens Neural Behav Physiol* 191: 715-732, 2005.
619 **Arbas EA, and Calabrese RL**. Ionic conductances underlying the activity of interneurons that control
620 heartbeat in the medicinal leech. *J Neurosci* 7: 3945-3952, 1987a.
621 **Arbas EA, and Calabrese RL**. Slow oscillations of membrane potential in interneurons that control
622 heartbeat in the medicinal leech. *J Neurosci* 7: 3953-3960, 1987b.
623 **Arshavsky Y, I., Deliagina TG, Orlovsky GN, Panchin YV, Pavlova GA, and Popova LB**. Control of
624 locomotion in marine mollusc Clione limacina. VI. Activity of isolated neurons of pedal ganglia.
625 *Experimental brain research* 63: 106-112, 1986.
626 **Arshavsky YI, Beloozerova IN, Orlovsky GN, Panchin YV, and Pavlova GA**. Control of locomotion in
627 marine mollusc Clione limacina. III. On the origin of locomotory rhythm. *Experimental brain research*
628 58: 273-284, 1985.
629 **Arshavsky YI, Deliagina TG, Orlovsky GN, Panchin YV, Popova LB, and Sadreyev RI**. Analysis of the
630 central pattern generator for swimming in the mollusk Clione. *Ann N Y Acad Sci* 860: 51-69, 1998.
631 **Brown TG**. The Intrinsic Factors in the Act of Progression in the Mammal. *Proc R Soc Lond B* 84: 308-319,
632 1911.
633 **Byrne JH, Castellucci VF, and Kandel ER**. Contribution of individual mechanoreceptor sensory neurons
634 to defensive gill-withdrawal reflex in Aplysia. *J Neurophysiol* 41: 418-431, 1978.
635 **Cymbalyuk GS, Gaudry Q, Masino MA, and Calabrese RL**. Bursting in leech heart interneurons: cell-
636 autonomous and network-based mechanisms. *J Neurosci* 22: 10580-10592, 2002.
637 **Daun S, Rubin JE, and Rybak IA**. Control of oscillation periods and phase durations in half-center central
638 pattern generators: a comparative mechanistic analysis. *Journal of computational neuroscience* 27: 3-
639 36, 2009.
640 **Destexhe A, Mainen ZF, and Sejnowski TJ**. An Efficient Method for Computing Synaptic Conductances
641 Based on a Kinetic Model of Receptor Binding. *Neural Comput* 6: 14-18, 1994.
642 **Dethier J, Drion G, Franci A, and Sepulchre R**. A positive feedback at the cellular level promotes
643 robustness and modulation at the circuit level. *J Neurophysiol* 114: 2472-2484, 2015.
644 **Friesen WO**. Reciprocal inhibition: a mechanism underlying oscillatory animal movements. *Neuroscience*
645 *and biobehavioral reviews* 18: 547-553, 1994.

646 **Friesen WO, and Stent GS**. Neural circuits for generating rhythmic movements. *Annu Rev Biophys*
647 *Bioeng* 7: 37-61, 1978.
648 **Grillner S**. The motor infrastructure: from ion channels to neuronal networks. *Nat Rev Neurosci* 4: 573-
649 586, 2003.
650 **Grillner S, and El Manira A**. The intrinsic operation of the networks that make us locomote. *Curr Opin*
651 *Neurobiol* 31: 244-249, 2015.
652 **Kemenes I, Marra V, Crossley M, Samu D, Staras K, Kemenes G, and Nowotny T**. Dynamic clamp with
653 StdpC software. *Nat Protoc* 6: 405-417, 2011.
654 **Kiehn O**. Decoding the organization of spinal circuits that control locomotion. *Nat Rev Neurosci* 17: 224-
655 238, 2016.
656 **Kiehn O, Johnson BR, and Raastad M**. Plateau properties in mammalian spinal interneurons during
657 transmitter-induced locomotor activity. *Neuroscience* 75: 263-273, 1996.
658 **Li WC, and Moult PR**. The control of locomotor frequency by excitation and inhibition. *J Neurosci* 32:
659 6220-6230, 2012.
660 **Li WC, Roberts A, and Soffe SR**. Specific brainstem neurons switch each other into pacemaker mode to
661 drive movement by activating NMDA receptors. *J Neurosci* 30: 16609-16620, 2010.
662 **Li WC, Sautois B, Roberts A, and Soffe SR**. Reconfiguration of a vertebrate motor network: specific
663 neuron recruitment and context-dependent synaptic plasticity. *J Neurosci* 27: 12267-12276, 2007.
664 **Liao X, and Walters ET**. The use of elevated divalent cation solutions to isolate monosynaptic
665 components of sensorimotor connections in Aplysia. *J Neurosci Methods* 120: 45-54, 2002.
666 **McCrea DA, and Rybak IA**. Organization of mammalian locomotor rhythm and pattern generation. *Brain*
667 *Res Rev* 57: 134-146, 2008.
668 **Moult PR, Cottrell GA, and Li WC**. Fast silencing reveals a lost role for reciprocal inhibition in
669 locomotion. *Neuron* 77: 129-140, 2013.
670 **Nagornov R, Osipov G, Komarov M, Pikovsky A, and Shilnikov AL**. Mixed-mode synchronization
671 between two inhibitory neurons with post-inhibitory rebound. *Comm Nonlinear Sci Num Sim* 36: 175-
672 191, 2016.
673 **Paulus W, and Rothwell JC**. Membrane resistance and shunting inhibition: where biophysics meets
674 state-dependent human neurophysiology. *J Physiol* 594: 2719-2728, 2016.
675 **Perkel DH, and Mulloney B**. Motor pattern production in reciprocally inhibitory neurons exhibiting
676 postinhibitory rebound. *Science* 185: 181-183, 1974.

677 **Pirtle TJ, and Satterlie RA**. The role of postinhibitory rebound in the locomotor central-pattern
678 generator of Clione limacina. *Integrative and comparative biology* 47: 451-456, 2007.
679 **Pirtle TJ, Willingham K, and Satterlie RA**. A hyperpolarization-activated inward current alters swim
680 frequency of the pteropod mollusk Clione limacina. *Comp Biochem Physiol A Mol Integr Physiol* 157:
681 319-327, 2010.
682 **Reith CA, and Sillar KT**. A role for slow NMDA receptor-mediated, intrinsic neuronal oscillations in the
683 control of fast fictive swimming in Xenopus laevis larvae. *Eur J Neurosci* 10: 1329-1340, 1998.
684 **Roberts A, Li WC, and Soffe SR**. Roles for inhibition: studies on networks controlling swimming in young
685 frog tadpoles. *J Comp Physiol A Neuroethol Sens Neural Behav Physiol* 194: 185-193, 2008.
686 **Rodriguez JC, Blitz DM, and Nusbaum MP**. Convergent rhythm generation from divergent cellular
687 mechanisms. *J Neurosci* 33: 18047-18064, 2013.
688 **Sakurai A, Gunaratne CA, and Katz PS**. Two interconnected kernels of reciprocally inhibitory
689 interneurons underlie alternating left-right swim motor pattern generation in the mollusc *Melibe*
690 *leonina*. *J Neurophysiol* 112: 1317-1328, 2014.
691 **Sakurai A, and Katz PS**. The central pattern generator underlying swimming in Dendronotus iris: a
692 simple half-center network oscillator with a twist. *J Neurophysiol* 116: 1728-1742, 2016.
693 **Sakurai A, and Katz PS**. Command or obey? Homologous neurons differ in hierarchical position for the
694 generation of homologous behaviors. *J Neurosci* 2019.
695 **Sakurai A, and Katz PS**. Spike timing-dependent serotonergic neuromodulation of synaptic strength
696 intrinsic to a central pattern generator circuit. *J Neurosci* 23: 10745-10755, 2003.
697 **Sakurai A, Newcomb JM, Lillvis JL, and Katz PS**. Different roles for homologous interneurons in species
698 exhibiting similar rhythmic behaviors. *Curr Biol* 21: 1036-1043, 2011.
699 **Selverston AI, and Miller JP**. Mechanisms underlying pattern generation in lobster stomatogastric
700 ganglion as determined by selective inactivation of identified neurons. I. Pyloric system. *J*
701 *Neurophysiol* 44: 1102-1121, 1980.
702 **Sharp AA, Skinner FK, and Marder E**. Mechanisms of oscillation in dynamic clamp constructed two-cell
703 half-center circuits. *J Neurophysiol* 76: 867-883, 1996.
704 **Tazerart S, Viemari JC, Darbon P, Vinay L, and Brocard F**. Contribution of persistent sodium current to
705 locomotor pattern generation in neonatal rats. *J Neurophysiol* 98: 613-628, 2007.
706 **Wallen P, and Grillner S**. N-methyl-D-aspartate receptor-induced, inherent oscillatory activity in neurons
707 active during fictive locomotion in the lamprey. *J Neurosci* 7: 2745-2755, 1987.

Wang XJ, and Rinzel J. Alternating and synchronous rhythms in reciprocally inhibitory model neurons. *Neural Computation* 4: 84-97, 1992.

Watson WH, 3rd, Newcomb JM, and Thompson SM. Neural correlates of swimming behavior in Melibe leonina. *The Biological bulletin* 203: 152-160, 2002.

Zhong G, Masino MA, and Harris-Warrick RM. Persistent sodium currents participate in fictive locomotion generation in neonatal mouse spinal cord. *J Neurosci* 27: 4507-4518, 2007.

Ziskind-Conhaim L, Wu L, and Wiesner EP. Persistent sodium current contributes to induced voltage oscillations in locomotor-related hb9 interneurons in the mouse spinal cord. *J Neurophysiol* 100: 2254-2264, 2008.

Figure 1

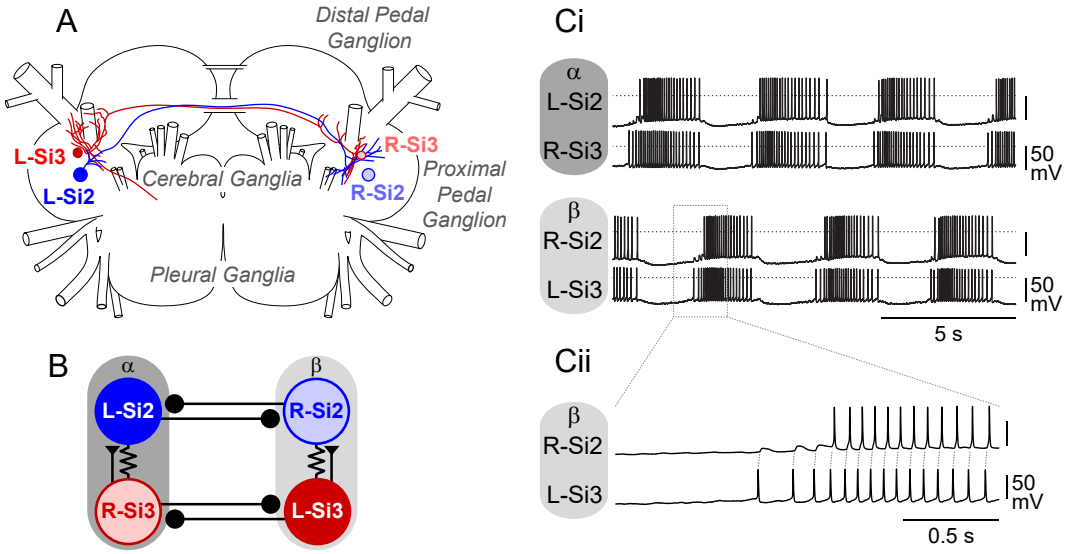
A
Distal Pedal Ganglion
L-Si3
L-Si2
Cerebral Ganglia
R-Si3
R-Si2
Proximal Pedal Ganglion
Pleural Ganglia
B
α
β
L-Si2
R-Si2
R-Si3
L-Si3
Ci
α
L-Si2
R-Si3
50 mV
β
R-Si2
L-Si3
50 mV
5 s
Cii
β
R-Si2
L-Si3
50 mV
0.5 s

Figure 2

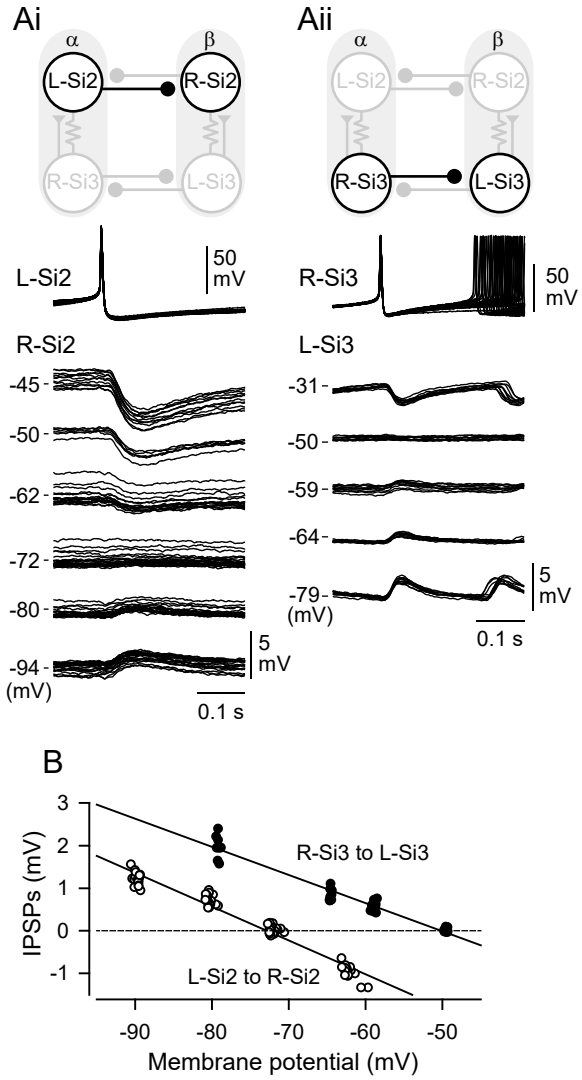
Ai
α
β
L-Si2
R-Si2
R-Si3
L-Si3
L-Si2
50 mV
R-Si2
-45
-50
-62
-72
-80
-94
(mV)
5 mV
0.1 s
Aii
α
β
L-Si2
R-Si2
R-Si3
L-Si3
R-Si3
50 mV
L-Si3
-31
-50
-59
-64
-79
(mV)
5 mV
0.1 s
B
IPSPs (mV)
3
2
1
0
-1
R-Si3 to L-Si3
L-Si2 to R-Si2
-90
-80
-70
-60
-50
Membrane potential (mV)

Figure 3

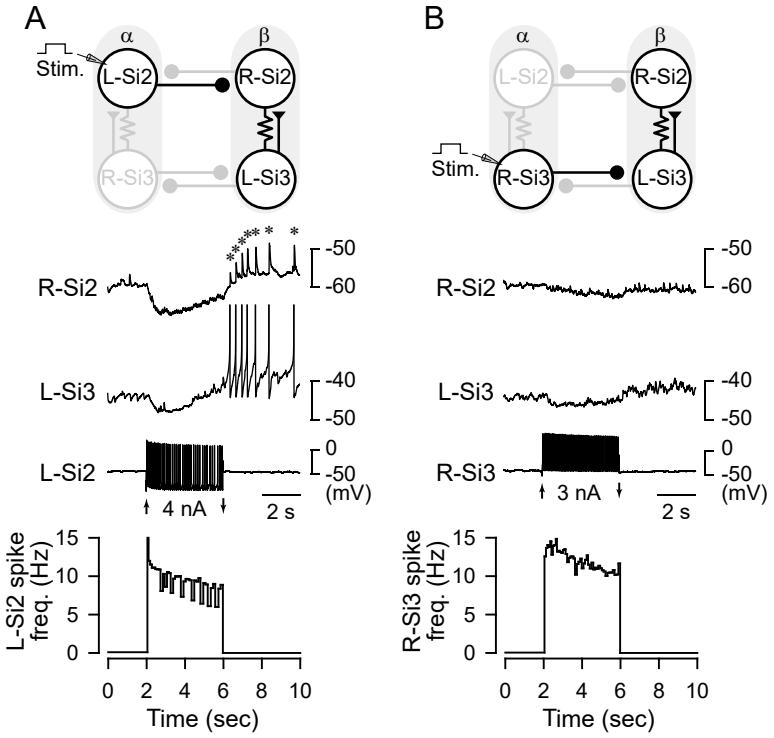
A
α
β
Stim.
L-Si2
R-Si2
R-Si3
L-Si3
R-Si2
-50
-60
L-Si3
-40
-50
L-Si2
0
-50
(mV)
4 nA
2 s
L-Si2 spike freq. (Hz)
15
10
5
0
0 2 4 6 8 10
Time (sec)
B
α
β
L-Si2
R-Si2
Stim.
R-Si3
L-Si3
R-Si2
-50
-60
L-Si3
-40
-50
R-Si3
0
-50
(mV)
3 nA
2 s
R-Si3 spike freq. (Hz)
15
10
5
0
0 2 4 6 8 10
Time (sec)

Figure 4

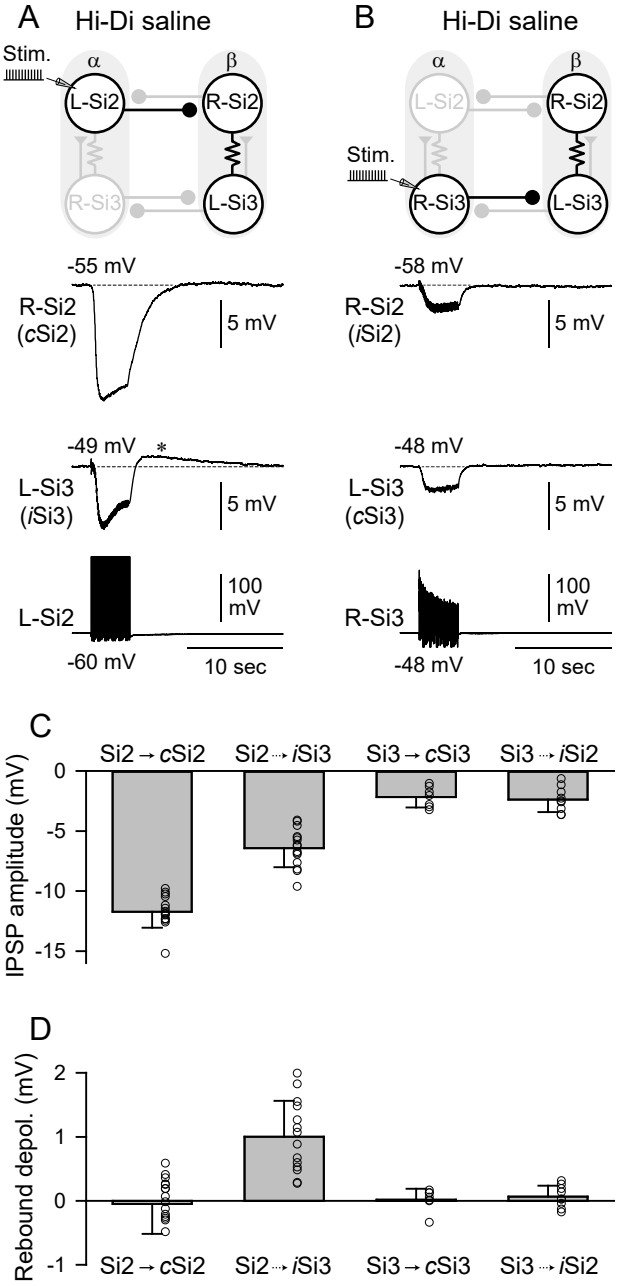
A
Hi-Di saline
Stim.
α
β
L-Si2
R-Si2
R-Si3
L-Si3
-55 mV
R-Si2
(cSi2)
5 mV
-49 mV
*
L-Si3
(iSi3)
5 mV
L-Si2
100
mV
-60 mV
10 sec
B
Hi-Di saline
α
β
L-Si2
R-Si2
Stim.
R-Si3
L-Si3
-58 mV
R-Si2
(iSi2)
5 mV
-48 mV
L-Si3
(cSi3)
5 mV
R-Si3
100
mV
-48 mV
10 sec
C
Si2 → cSi2
Si2 ⇢ iSi3
Si3 → cSi3
Si3 ⇢ iSi2
IPSP amplitude (mV)
0
-5
-10
-15
D
Rebound depol. (mV)
2
1
0
-1
Si2 → cSi2
Si2 ⇢ iSi3
Si3 → cSi3
Si3 ⇢ iSi2

Figure 5

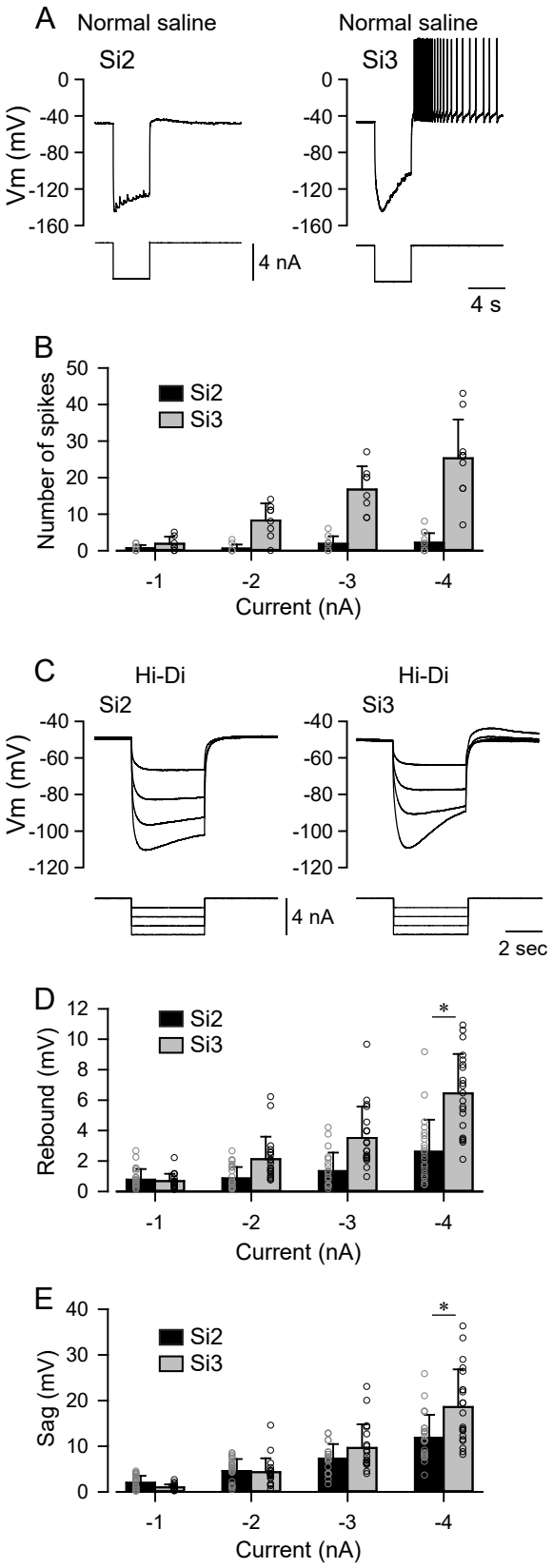
A
Normal saline
Si2
Normal saline
Si3
Vm (mV)
0
-40
-80
-120
-160
4 nA
4 s
B
Number of spikes
50
40
30
20
10
0
Si2
Si3
-1
-2
-3
-4
Current (nA)
C
Hi-Di
Si2
Hi-Di
Si3
Vm (mV)
-40
-60
-80
-100
-120
4 nA
2 sec
D
Rebound (mV)
12
10
8
6
4
2
0
Si2
Si3
*
-1
-2
-3
-4
Current (nA)
E
Sag (mV)
40
30
20
10
0
Si2
Si3
*
-1
-2
-3
-4
Current (nA)

Figure 6

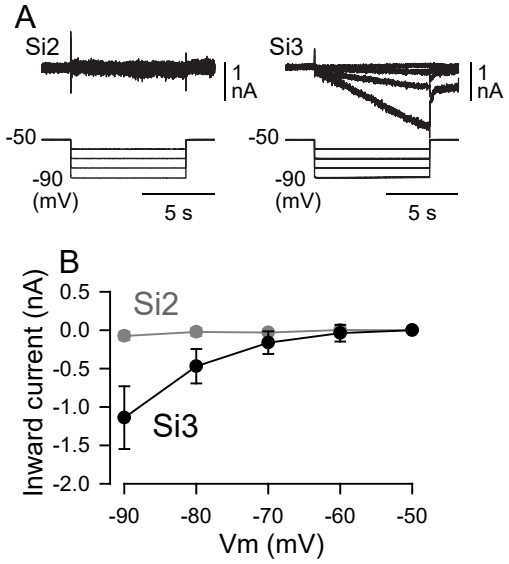
A
Si2
1
nA
-50
-90
(mV)
5 s
Si3
1
nA
-50
-90
(mV)
5 s
B
Inward current (nA)
0.5
0.0
-0.5
-1.0
-1.5
-2.0
Si2
Si3
-90
-80
-70
-60
-50
Vm (mV)

Figure 7

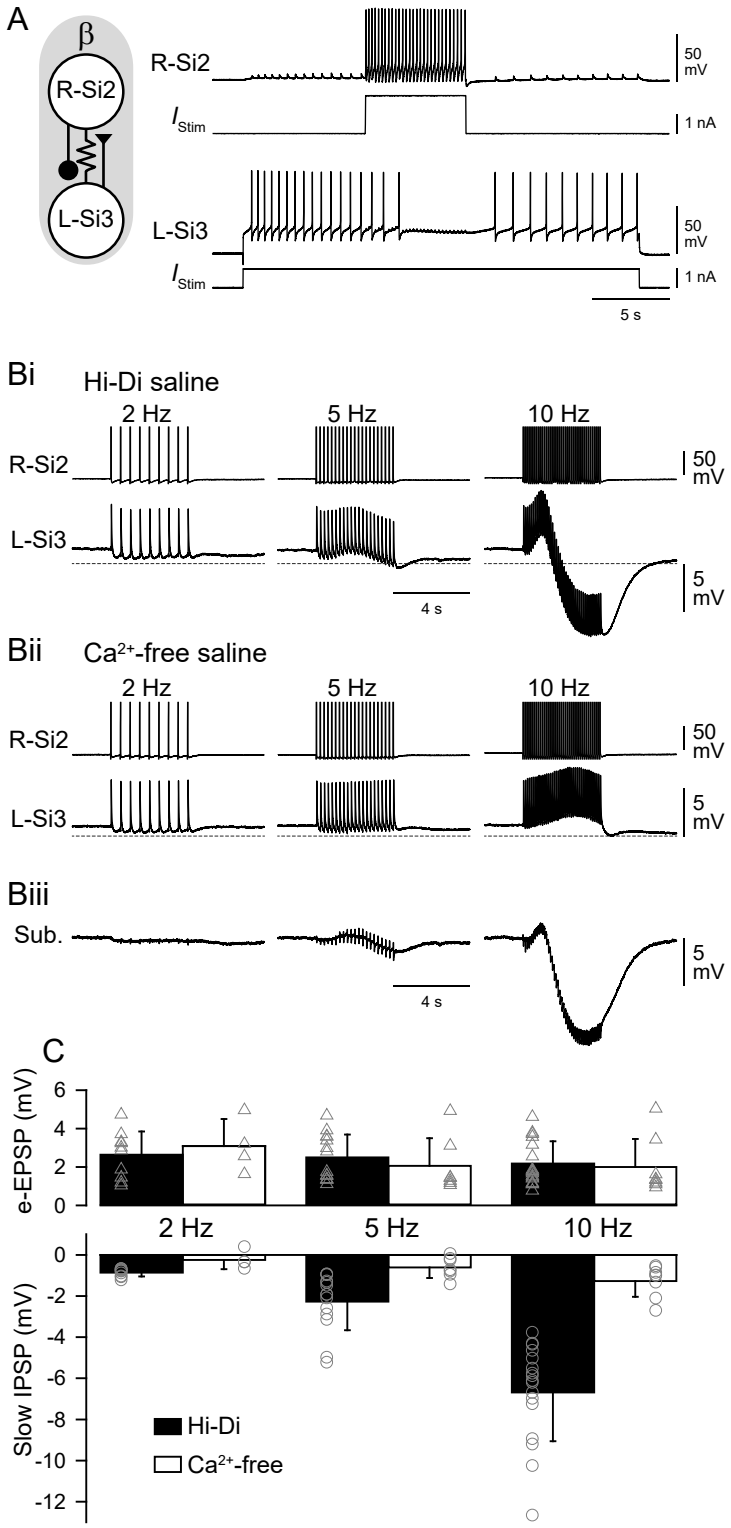
A
β
R-Si2
L-Si3
R-Si2
I_{Stim}
L-Si3
I_{Stim}
50 mV
1 nA
50 mV
1 nA
5 s
Bi
Hi-Di saline
2 Hz
5 Hz
10 Hz
R-Si2
L-Si3
50 mV
5 mV
4 s
Bii
Ca²⁺-free saline
2 Hz
5 Hz
10 Hz
R-Si2
L-Si3
50 mV
5 mV
Biii
Sub.
5 mV
4 s
C
e-EPSP (mV)
6
4
2
0
2 Hz
5 Hz
10 Hz
Slow IPSP (mV)
0
-2
-4
-6
-8
-10
-12
Hi-Di
Ca²⁺-free

Figure 8

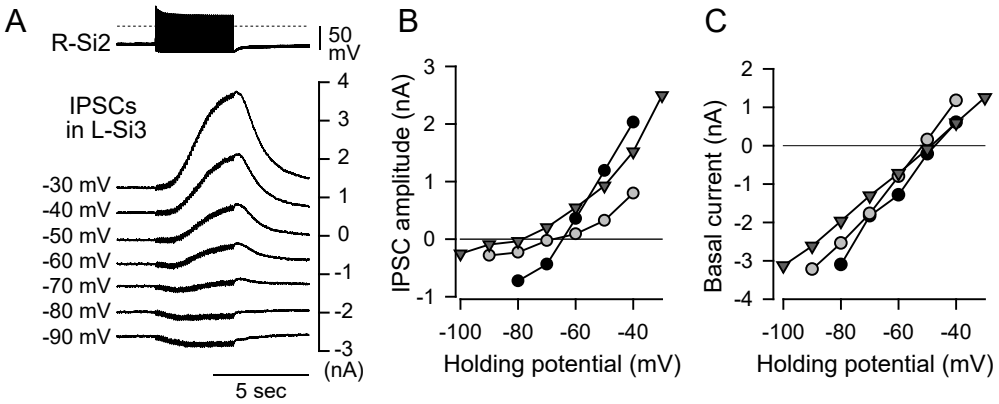
A
R-Si2
50 mV
IPSCs in L-Si3
-30 mV
-40 mV
-50 mV
-60 mV
-70 mV
-80 mV
-90 mV
4
3
2
1
0
-1
-2
-3
(nA)
5 sec
B
IPSC amplitude (nA)
3
2
1
0
-1
-100
-80
-60
-40
Holding potential (mV)
C
Basal current (nA)
2
1
0
-1
-2
-3
-4
-100
-80
-60
-40
Holding potential (mV)

Figure 9

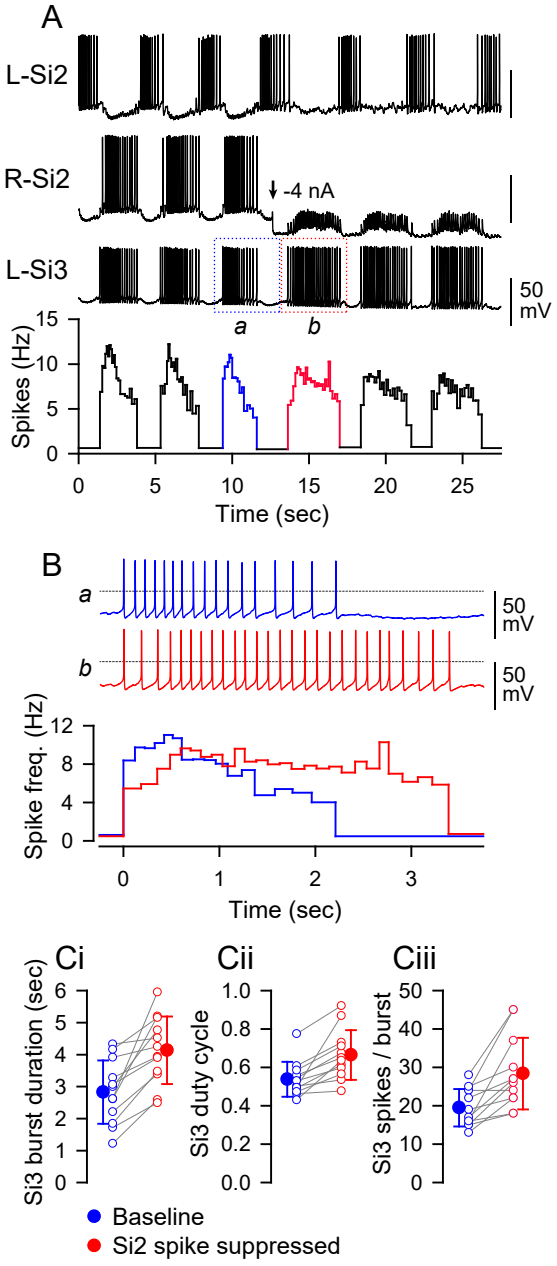
A
L-Si2
R-Si2
-4 nA
L-Si3
50 mV
a
b
Spikes (Hz)
15
10
5
0
0
5
10
15
20
25
Time (sec)
B
a
b
50 mV
50 mV
Spike freq. (Hz)
12
8
4
0
0
1
2
3
Time (sec)
Ci
Cii
Ciii
Si3 burst duration (sec)
Si3 duty cycle
Si3 spikes / burst
Baseline
Si2 spike suppressed

Figure 10

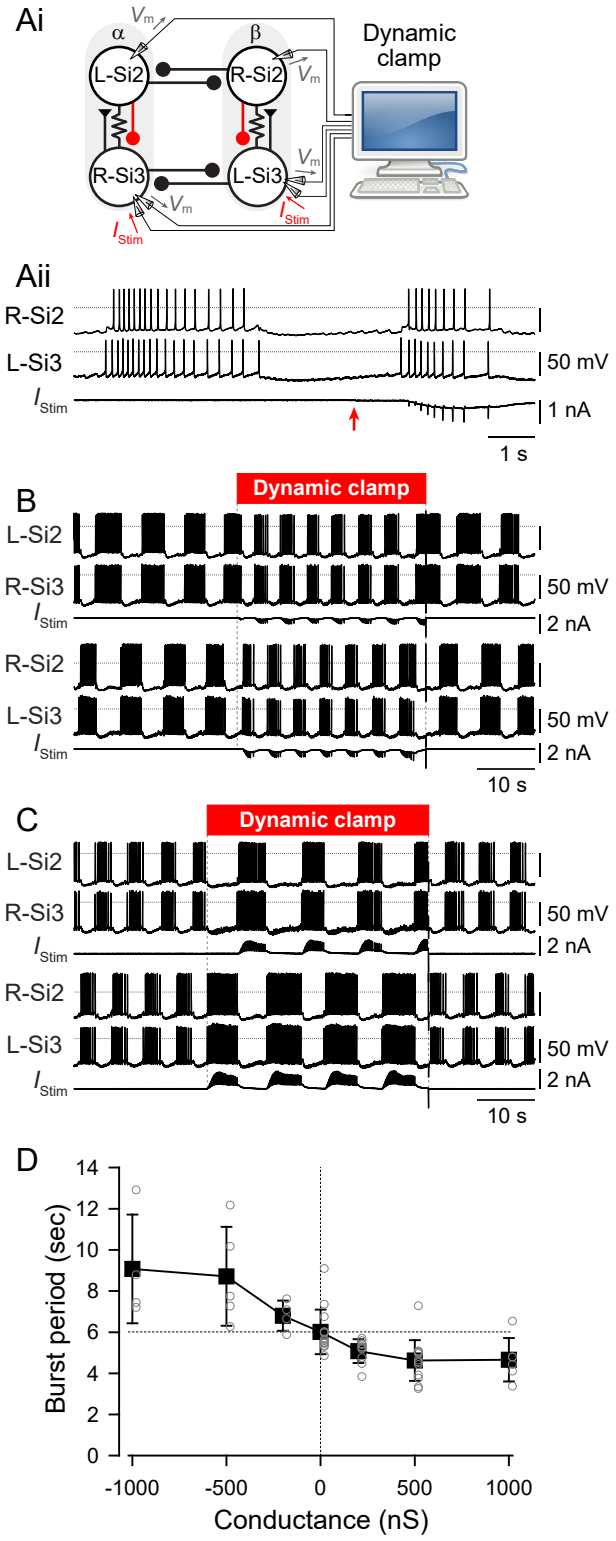
Ai
α
β
L-Si2
R-Si2
R-Si3
L-Si3
Vm
Istim
Dynamic clamp
Aii
R-Si2
L-Si3
Istim
50 mV
1 nA
1 s
B
Dynamic clamp
L-Si2
R-Si3
Istim
R-Si2
L-Si3
50 mV
2 nA
10 s
C
Dynamic clamp
L-Si2
R-Si3
Istim
R-Si2
L-Si3
50 mV
2 nA
10 s
D
Burst period (sec)
Conductance (nS)
0
2
4
6
8
10
12
14
-1000
-500
0
500
1000
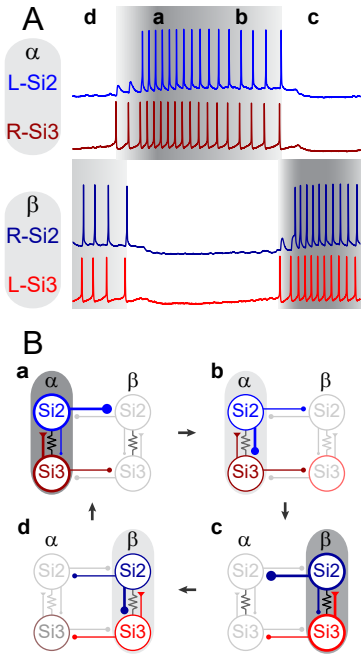
Figure 11